Journal of Materials Chemistry A

Accepted Manuscript

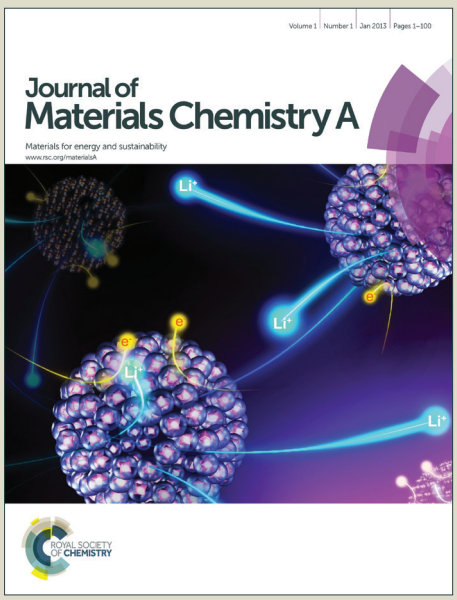

ROYAL SOCIETY OF CHEMISTRY

www.rsc.org/materialsA

A table of contents entry

We present a novel method to grow uniform Cl-incorporated perovskite absorber layer using mixed halide source by modified two-step process.

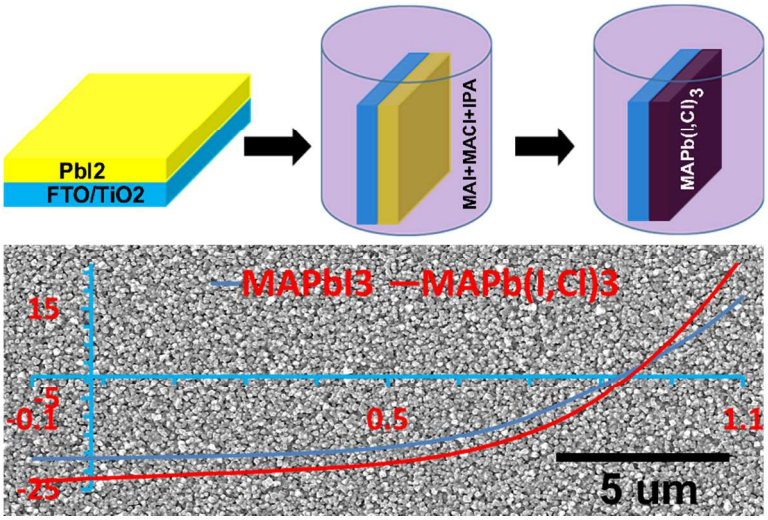

Journal of Materials Chemistry A

Cite this: DOI: 10.1039/c0xx00000x

ARTICLE TYPE

www.rsc.org/xxxxxx

Enhancing the performance of planar organo-lead halide perovskite solar cells by using mixed halide source

Minlin Jiang,[a] Jiamin Wu,[b] Fei Lan,[a] Quan Tao,[a] Di Gao*[b] and Guangyong Li*[a]

Received (in XXX, XXX) Xth XXXXXXXXX 20XX, Accepted Xth XXXXXXXXX 20XX

DOI: 10.1039/b000000x

Cl incorporation has benn reported to be able to significantly increase the diffusion length of carriers in organo-lead halide perovskite thin films. However, due to the low solubility of $PbCl_2$, Cl incorporation has been rarely reported in the two-step process, a process capable of producing uniform organo-lead halide perovskite thin films. In this letter, we report a novel growth method that combines the two-step process and the Cl incorporation. The Cl-incorporated organo-lead halide perovskite solar cell made from two-step process demonstrated a power conversion efficiency of 10.5%, which is 27% higher than that without Cl incorporation. Further investigation has been performed to explore the fundamentals for the enhancement. Kelvin probe force microscopy (KPFM) measurement revealed a larger band bending at grain boundaries with Cl incorporation, which brings the Fermi level of the bulk perovskite thin film closer to the center of the bandgap. As a result, a p-i-n type of junction is formed in the devices with Cl incorporation, which facilitates the charge carrier collection. Additional carrier lifetime measurement indicates that the electron lifetime in perovskite thin film with Cl incorporation is longer, indicating a reduced recombination in the devices with Cl incorporation.

Introduction

Methylammonium lead halide perovskites have emerged as promising photovoltaic (PV) materials because of their excellent optical properties such as high absorption coefficients for a broad range of sunlight absorption.[1] Also, the abundance of raw materials and the ability of being solution processed make methylammonium lead halide perovskites more suitable for low cost PV technologies. High power conversion efficiencies of more than 15% have been reported from both mesoporous structure devices and planar structure devices.[1-5] The planar structure devices are more advantageous than the mesoporous structure devices because high temperature annealing necessary for mesorporous structure is not required for planar structure devices. Thus, low temperature processing, which is suitable for plastic solar cells, can be applied to fabricate methylammonium lead halide perovskite solar cells. Conversion efficiency in excess of 10% has been reported for methylammonium lead halide perovskite solar cell fabricated on plastic substrates.[3]

So far, two processes have been developed to fabricate planar perovskite solar cells. The first process is called one-step process where metal halide is mixed with methylammonium iodide and the as-synthesized methylammonium lead halide perovskite is spin-coated on substrates. The other process is called two-step process where metal halide is spin-coated on substrates and methylammonium lead halide perovskite is formed by inserting the substrates into methylammonium iodide solution. In one-step process, two metal halides, lead iodide (PbI_2) and lead chloride ($PbCl_2$), have been commonly used to synthesize methylammonium lead halide perovskites which are denoted as $MAPbI_3$ and $MAPb(I,Cl)_3$, respectively, with $MAPb(I,Cl)_3$ solar cells leading the performance due to its long diffusion length of carriers.[6, 7] Nevertheless, it is extremely difficult to control the morphology of perovskite thin films because it is significantly affected by the environment of one-step process.[8] In two-step process, the morphology of perovskite thin film is very uniform.[3] However, PbI_2 has been exclusively used because the solubility of $PbCl_2$ is extremely low. Therefore, the advantages associated with Cl incorporation cannot be taken.

In this paper, we report a novel two-step growth method which combines the Cl incorporation by using mixed halide source. It is found that the short current density (J_{SC}) has been significantly improved by 28% after Cl incorporation. As a result, power conversion efficiency (PCE) of 10.5% was obtained from solution-processed planar perovskite solar cell.

Results and discussion

Planar perovskite solar cells were fabricated in air with a structure of FTO/TiO_2/perovskite/spiro-MeOTAD/Au. A

modified two-step process capable of incorporating Cl is used to grow the perovskite thin films. The experimental procedures for two-step growth are briefly shown in Fig. 1. First, PbI_2 solution (dissolved in N,N-dimethylformamide (DMF) with a concentration of 460 mg/ml) was spin coated at 4000 RPM for 30s. After dried in air, the substrates with PbI_2 thin film were separated into two batches. The first batch was dipped into solution containing single halide source (CH_3NH_3I (MAI) dissolved in 2-propanol (IPA) with a concentration of 20 mg/ml). These samples were denoted as $MAPbI_3$. The second batch was dipped into solution containing mixed halide source (MAI and CH_3NH_3Cl (MACl) dissolved in 2-propanol with concentrations of 20 mg/ml and 2 mg/ml, respectively). These samples were named as $MAPb(I,Cl)_3$.

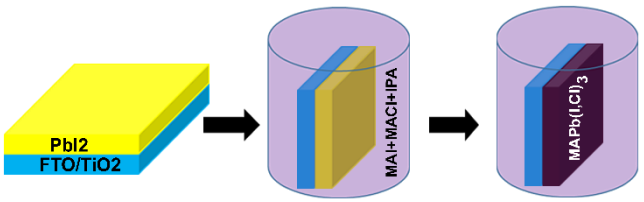

Fig. 1 Schematic growth process for perovskite thin films using mixed halide source.

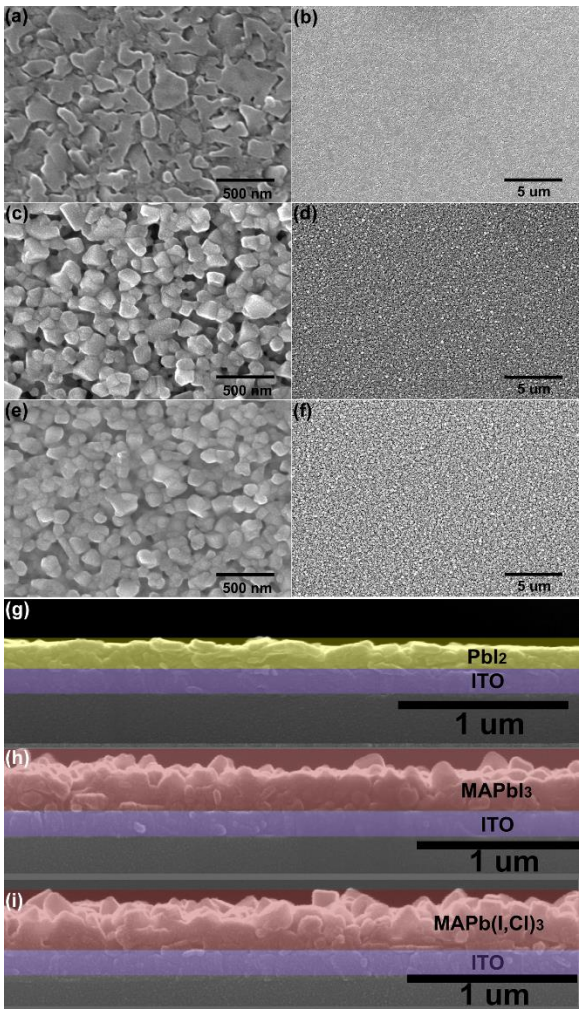

Fig. 2 SEM images of PbI_2 (a, b, and g), $MAPbI_3$ (c, d, and h), and $MAPb(I,Cl)_3$ (e, f, and i) thin films.

The content of Cl has been checked by energy-dispersive X-ray spectroscopy (EDS). The EDS spectra of $MAPb(I,Cl)_3$ and $MAPbI_3$ thin films are shown in Fig. S1. The weight ratios of Pb, I, and Cl derived from the EDS spectra are summarized in Table S1. The weight ratios of Cl in $MAPb(I,Cl)_3$ and $MAPbI_3$ thin films are same. This indicates that the concentration of Cl in $MAPb(I,Cl)_3$ should be lower than the detection limit of the EDS system because no Cl has been intentionally added to the so-called $MAPbI_3$ thin film.

The PbI_2 thin film is continuous and the substrate is fully covered by the PbI_2 thin film as shown in Fig. 2a and 2b. It is evident that the PbI_2 thin film consists of crystals with sizes varying from tens to a few hundred nanometers. The reaction between PbI_2 and MAI is efficient due to the ordered crystal structure of PbI_2 thin film which facilitates the intercalation of MAI into the lattice to form $MAPbI_3$. The SEM images of the surfaces of $MAPbI_3$ and $MAPb(I,Cl)_3$ thin films are shown in Fig. 2 (c-f). Due to the uniformity of PbI_2 thin film, which possibly modifies the interaction between the substrate and the perovskite thin film, the resulted perovskite thin films are homogeneous and densely packed. This demonstrates the advantage of two-step process for preparing perovskite thin films, comparing to the one-step process which usually leads to incomplete coverage of substrate.[8] In the case of $MAPb(I,Cl)_3$ thin film that was prepared using mixed halide source, no difference is observed in the morphology, indicating the addition of MACl does not affect the growth of perovskite thin film and the interaction between the substrate and the perovskite thin film. The SEM cross-section images of the PbI_2, $MAPbI_3$, and $MAPb(I,Cl)_3$ thin films are shown in Fig. 2 (g), (h), and (i), respectively. There is no region with complete absence of absorber. This prevents the shunting path that is partially responsible for the lower fill factor and open-circuit voltage in the one-step processed perovskite solar cells.

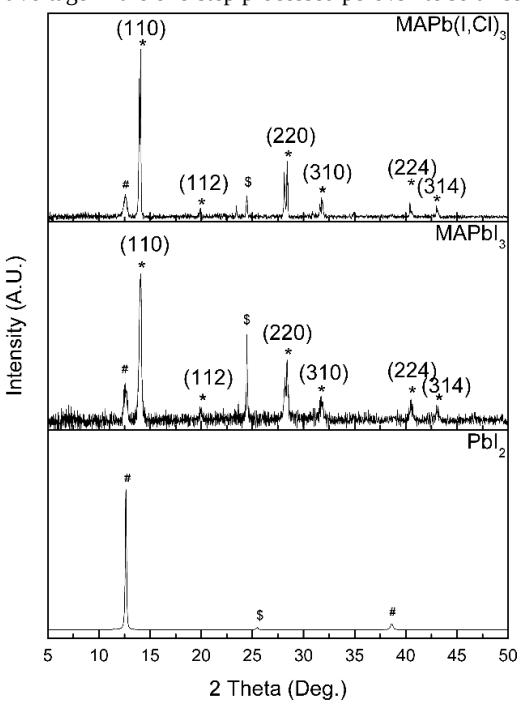

Fig. 3 XRD patterns of PbI_2, $MAPbI_3$, and $MAPb(I,Cl)_3$ thin films. Peaks associated with the perovskite, the PbI_2, and the TiO_2 are labelled (* is for perovskite structure, # is for PbI_2, and $ is for TiO_2).

XRD patterns of PbI_2, $MAPbI_3$, and $MAPb(I,Cl)_3$ thin films are shown in Fig. 3. A strong diffraction peak at 12.63° is observed for PbI_2 thin film. This corresponds to the (001) lattice plane of crystallized PbI_2, indicating the polycrystalline nature of deposited PbI_2 thin film.[1, 9] Both $MAPbI_3$ and $MAPb(I,Cl)_3$ thin films demonstrate a comparatively strong diffraction peak at 14.07° which corresponds to the tetragonal structured perovskite.[10] The similarity of XRD patterns indicates the growth of perovskite thin film is not structurally affected by the addition of MACl. For $MAPbI_3$ and $MAPb(I,Cl)_3$ thin films, the PbI_2 diffraction peak at 12.63° still exists besides the perovskite diffractions, indicating the PbI_2 was not fully converted into perovskite.

The J-V curves (under 100 mW/cm^2 AM1.5G illumination) of the best perovskite solar cells are shown in Fig. 4, and the PV parameters are summarized in Table 1. The most efficient $MAPbI_3$ solar cell has a short-circuit current density (J_{SC}) of 17.60 mA/cm^2, an open-circuit voltage (V_{OC}) of 0.90 V and a fill factor (FF) of 52 %, yielding an efficiency (η) of 8.29 %. The best $MAPb(I,Cl)_3$ solar cell produced a J_{SC} of 22.58 mA/cm^2, an V_{OC} of 0.91V and a FF of 51 %, resulting an overall efficiency of 10.49 %. The improvement of performance mainly comes from the significant enhancement in J_{SC} which is improved by 28 %. This improved J_{SC} cannot be attributed to stronger light absorption because $MAPb(I,Cl)_3$ thin film had similar absorption spectrum with that of $MAPbI_3$ thin film as shown in Fig. 2S. This could be attributed to the long diffusion length of carriers in $MAPb(I,Cl)_3$ thin film. The averaged I-V parameters are summarized in Table S2. While the best $MAPbI_3$ and $MAPb(I,Cl)_3$ solar cells demonstrated comparable V_{OC}, higher averaged V_{OC} was obtained from $MAPb(I,Cl)_3$ solar cells.

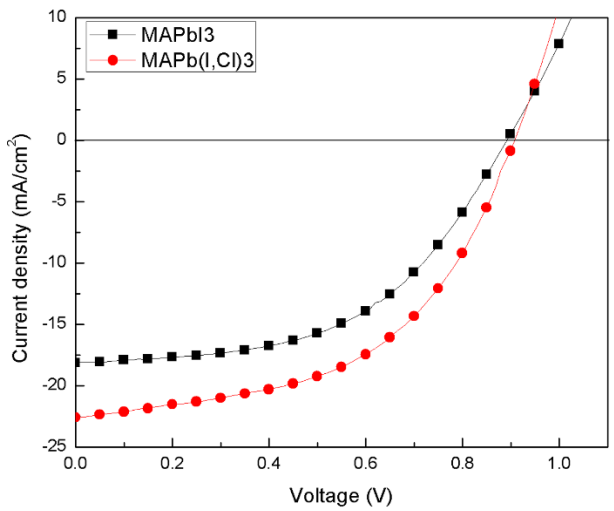

Fig. 4 J–V curves of the best perovskite solar cells.

Table 1 I-V parameters of the best perovskite solar cells

	V_{OC} (V)	J_{SC}(mA/cm^2)	FF(%)	η(%)
$MAPbI_3$	0.90	17.60	0.52	8.29
$MAPb(I,Cl)_3$	0.91	22.58	0.51	10.49

To investigate the mechanisms behind the significant improvement in the performance of $MAPb(I,Cl)_3$ solar cells, the surface potential (SP) distributions of both materials were mapped using single-pass Kelvin probe force microscopy (KPFM).[11] As shown in Fig. 5, the dark regions around grain boundaries indicate the band bending that favour electron accumulation. KPFM measurement of $MAPbI_3$ shows a uniform distribution of SP among grain bodies and grain boundaries indicating a narrower and smaller band bending, while KPFM measurement of $MAPb(I,Cl)_3$ shows a large variation of SP among grain bodies and grain boundaries indicating a deeper and wider band bending at the grain boundaries .

$MAPbI_3$ was found to be a p-type material,[1] thus a single p-n heterojunction should be formed at the cathode side of the device (Fig. 6a). For this single p-n heterojunction, an electron blocking layer is needed on the anode side. The charge collection efficiency is higher on the junction side (cathode) but lower on the anode side because only diffusion contributes to the charger transport on the anode side. The observation of wider and deeper band bending at the grain boundaries of $MAPb(I,Cl)_3$ from KPFM measurements indicates that electron accumulation is enhanced at the grain boundaries thus bring the Fermi level closer to the center band to make $MAPb(I,Cl)_3$ less p-type. Such Fermi level shift results in a p-i-n heterojunction in the device (Fig. 6b), first speculated in mesoporous $MAPb(I,Cl)_3$ solar cells[12] and later observed in planar $MAPb(I,Cl)_3$ solar cells by electron beam-induced current study.[13] The p-i-n heterojunction facilitates the charge collection on both sides because both drift and diffusion contribute to the charge transport. In addition, the junction on the anode side provides a blocking barrier to prevent electrons reaching the anode, thus to reduce recombination loss.

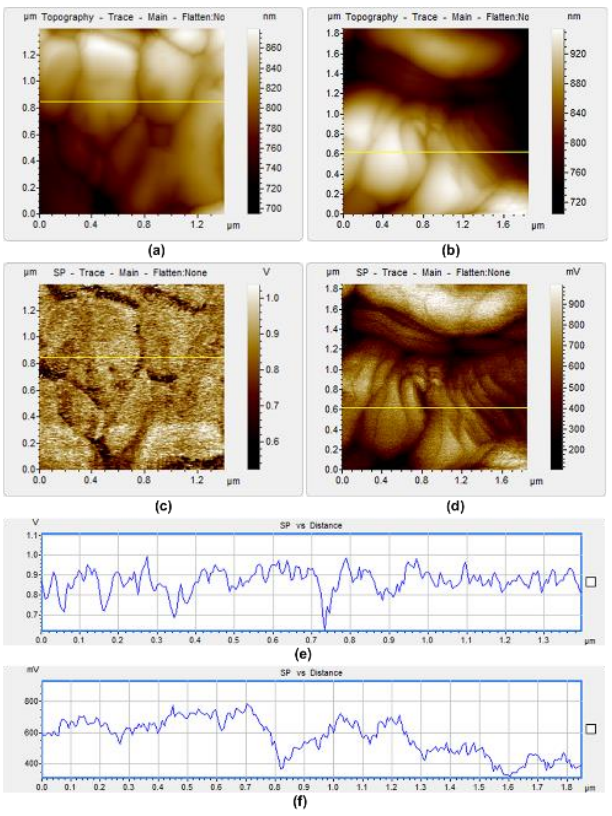

Fig. 5 Topography AFM images (a and b), SP (c and d), and profiles of SP (e and f) of $MAPbI_3$ (a, c, and e) and $MAPb(I,Cl)_3$ (b, d, and f) thin films on ITO.

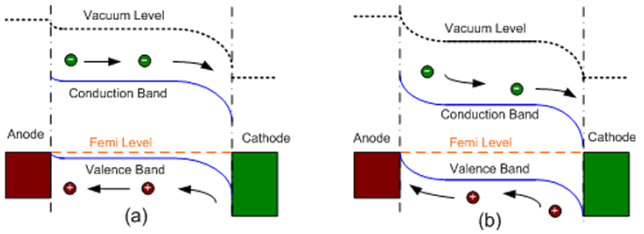

Fig. 6 Band alignment of devices for (a) $MAPbI_3$ and (b)$MAPb(I,Cl)_3$.

The measurement of electron lifetime can be applied to quantify the extent of electron recombination in perovskite solar cells.[14] The dependence of electron lifetime on the V_{OC} for planar perovskite solar cells fabricated with single and mixed halide source is shown in Fig. 7. It clearly demonstrates that the electron lifetime of the $MAPb(I,Cl)_3$ solar cells is longer than that of the $MAPbI_3$ solar cell. This suggests that the electrons in $MAPb(I,Cl)_3$ thin film can survive longer and demonstrate a longer diffusion length as reported in literatures.[6, 7]

The longer electron lifetime in $MAPb(I,Cl)_3$ solar cells, indicating a reduced recombination, can also be explained by the KPFM observation. The lack of SP difference at grain boundaries and grain bulk of $MAPbI_3$ may render free carriers generated during illumination to easily recombine, thus shorten carrier lifetime. On the contrary, the large variation of SP between grain boundary and grain bulk means abundant potential wells are formed at the grain boundaries to accommodate electrons, which physically separate electrons from holes preventing the carrier recombination. In addition, the locally formed junctions between the grain bodies and grain boundaries enhance the dissociation of excitons and further suppress recombination. As a result, carrier life time is greatly improved in $MAPb(I,Cl)_3$ solar cells.

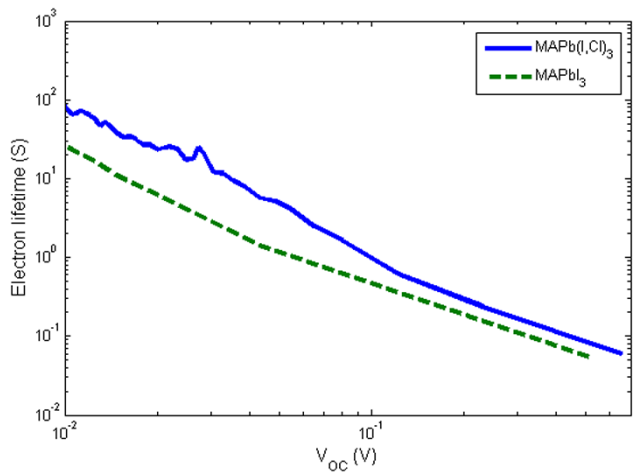

Fig. 7 The electron lifetime as a function of V_{OC}.

Photocurrent hysteresis has been reported in perovskite devices, which strongly depends on the fabrication processes, the scanning rate and the direction of voltage applied during I-V characterization.[1] In order to truly reflect the I-V performance of the perovskite solar cells reported in this work, the voltage was swept from either from -0.1V to 1.1V (forward bias) or from 1.1V to -0.1V (reverse bias) at a rate of 10 mV/s with a step of 10 mV/step. As shown in Fig. S3, no obvious hysteresis was observed in the I-V curve by changing the sweeping direction of voltage.

Although the efficiency of perovskite solar cells obtained in this work is not high compared with those reported in literatures,[1-5] there are still plenty of rooms to improve. The comparatively low performance could possibly be attributed to the incomplete conversion of PbI_2 as confirmed by the XRD results. Attempt to reduce the residue PbI_2 is still on-going in our research. Furthermore, the novel growth method for perovskite thin film proposed in this work could further improve the performance of perovskite solar cells by utilizing other techniques, such as using DMSO to dissolve PbI_2 and interdiffusion process as suggested in literatures[1,9]. Considering the devices were fabricated using solution process in atmosphere, our method should be promising for low-cost PV technologies.

Conclusions

The mixed halide source method proposed in this work can be applied to combine the advantages of two-step process and Cl incorporation. A larger band bending at grain boundaries with Cl incorporation, revealed by KPFM measurement, suggest that a p-i-n type of heterojunction junction is formed in the devices with Cl incorporation. The p-i-n junction facilitates the charge carrier collection and reduces recombination. Planar perovskite solar cells with uniform morphology can be fabricated by the two-step solution process and the performance can be improved by the Cl incorporation. This technique can be easily combined with other highly efficient growth methods. Higher performance could be expected for solution-processed, planar perovskite solar cells.

Experimental procedures

Synthesis of CH_3NH_3I and CH_3NH_3Cl

CH_3NH_3I and CH_3NH_3Cl were synthesized according to a reported procedure.[5] CH_3NH_3I was synthesized by reacting 30 mL of methylamine (40 % in methanol, TCI) and 32.3 mL of hydroiodic acid (57 wt% in water, Aldrich) in an ice bath for 2 h with stirring. The precipitate was collected through removing the solvents by a rotary evaporator. The as-obtained product was washed three times with diethyl ether, and then recrystallized from a mixed solvent of diethyl ether and ethanol. After filtration, the final CH_3NH_3I was collected and dried at 60 °C in a vacuum oven for 24 h. CH_3NH_3Cl was synthesized by reacting 30 mL of methylamine (40 % in methanol, TCI) and 20.4 mL of hydrochloric acid (37 wt% in water, Aldrich) in an ice bath for 2 h with stirring. The precipitation and collection of CH_3NH_3Cl was carried out using as same procedures as used for CH_3NH_3I.

Fabrication of perovskite solar cells

PbI_2 (1M) was dissolved in DMF and spin coated on patterned TiO_2-coated FTO glass substrates at 4000 RPM for 30 s. After being dried on a hotplate at 70 °C for 30 min, the samples were separated into two batches. The first batch was dipped into solution containing single halide source (CH_3NH_3I dissolved in 2-propanol (IPA) with a concentration of 20 mg/ml). These samples were denoted as $MAPbI_3$. The second batch was dipped into solution containing mixed halide source (CH_3NH_3I and CH_3NH_3Cl dissolved in IPA with concentrations of 20 mg/ml and 2 mg/ml, respectively). These samples were named as

$MAPb(I,Cl)_3$. The dipping was kept for 5 min. The samples were washed by IPA and then heated at 100 °C for 30 min. A layer of electron blocking material based on spiro-OMeTAD (80 mg spiro-OMeTAD, 29 μL tBP and 18 μL Li-TFSI solution (520 mg Li-TFSI in 1 mL acetonitrile) all dissolved in 1 mL chlorobenzene) was deposited on perovskite thin film by spin-coating at 4000 RPM for 30 s. Please note all the processes mentioned above were carried out in air. Finally, a gold layer with a thickness of 100 nm was deposited by electron beam evaporation with a mask. The active area of perovskite solar cells was 4 mm^2 which was defined by the overlap of Au and FTO layers and scribed to separate from the surrounding area.

Characterization

A UV-visible spectrometer (Agilent 8453) was used to obtain the absorbance of perovskite thin films. SEM images were taken from a scanning electron microscope (Philips XL30-FEG). X-ray diffraction (XRD) spectra were taken from a XRD system (PANalytical X'Pert Pro MRD) which was equipped with a CuKα1 X-ray generator. Current−voltage responses were measured using an Agilent 4155C semiconductor parameter analyzer under airmass 1.5 global (AM1.5G) 1 sun (100 mW/cm^2) illumination which was calibrated using a light intensity meter. No mask was applied during the I-V characterization. The voltage was swept from -0.1 V to 1.1 V at a rate of 10 mV/s with a step of 10 mV/step. For the hysteresis investigation, the voltage was swept from either from -0.1 V to 1.1 V (forward bias) or from 1.1 V to -0.1 V (reverse bias) at a rate of 10 mV/s with a step of 10 mV/step. KPFM measurement was carried out using Agilent 5500 AFM with MAC III mode. The conductive AFM tip (Veeco SCM-PIT, k=2.8 N/m, coated with Pt/Ir) was simultaneously excited by mechanical drive at its resonant frequency (75 kHz), and by electrical drive around 10 kHz.

Acknowledgements

This work was partially supported by the National Science Foundation (grants CBET 0967722 and CBET 1132819).

Notes and references

[a] *The Department of Electrical and Computer Engineering, University of Pittsburgh, Pittsburgh, PA 15261, USA. Fax: 412-624-8003; Tel: 412-624-9663; E-mail: gul6@pitt.edu*
[b] *The Department of Chemical and Petroleum Engineering, University of Pittsburgh, Pittsburgh, PA 15261, USA. Tel: 412-624-8488; E-mail: gaod@pitt.edu*

1. Z. G. Xiao, C. Bi, Y. C. Shao, Q. F. Dong, Q. Wang, Y. B. Yuan, C. G. Wang, Y. L. Gao and J. S. Huang, *Energ Environ Sci*, 2014, **7**, 2619-2623.
2. H. P. Zhou, Q. Chen, G. Li, S. Luo, T. B. Song, H. S. Duan, Z. R. Hong, J. B. You, Y. S. Liu and Y. Yang, *Science*, 2014, **345**, 542-546.
3. D. Y. Liu and T. L. Kelly, *Nat Photonics*, 2014, **8**, 133-138.
4. M. Z. Liu, M. B. Johnston and H. J. Snaith, *Nature*, 2013, **501**, 395-398.
5. J. Burschka, N. Pellet, S. J. Moon, R. Humphry-Baker, P. Gao, M. K. Nazeeruddin and M. Gratzel, *Nature*, 2013, **499**, 316-320.
6. S. D. Stranks, G. E. Eperon, G. Grancini, C. Menelaou, M. J. P. Alcocer, T. Leijtens, L. M. Herz, A. Petrozza and H. J. Snaith, *Science*, 2013, **342**, 341-344.
7. G. C. Xing, N. Mathews, S. Y. Sun, S. S. Lim, Y. M. Lam, M. Gratzel, S. Mhaisalkar and T. C. Sum, *Science*, 2013, **342**, 344-347.
8. G. E. Eperon, V. M. Burlakov, P. Docampo, A. Goriely and H. J. Snaith, *Adv Funct Mater*, 2014, **24**, 151-157.
9. Y. Z. Wu, A. Islam, X. D. Yang, C. J. Qin, J. Liu, K. Zhang, W. Q. Peng and L. Y. Han, *Energ Environ Sci*, 2014, **7**, 2934-2938.
10. A. T. Barrows, A. J. Pearson, C. K. Kwak, A. D. F. Dunbar, A. R. Buckley and D. G. Lidzey, *Energ Environ Sci*, 2014, **7**, 2944-2950.
11. F. Lan and G. Y. Li, *Nano Lett*, 2013, **13**, 2086-2091.
12. J. M. Ball, M. M. Lee, A. Hey and H. J. Snaith, *Energ Environ Sci*, 2013, **6**, 1739-1743.
13. E. Edri, S. Kirmayer, A. Henning, S. Mukhopadhyay, K. Gartsman, Y. Rosenwaks, G. Hodes and D. Cahen, *Nano Lett*, 2014, **14**, 1000-1004.
14. A. Zaban, M. Greenshtein and J. Bisquert, *Chemphyschem*, 2003, **4**, 859-864.
15. H. J. Snaith, A. Abate, J. M. Ball, G. E. Eperon, T. Leijtens, N. K. Noel, S. D. Stranks, J. T. W. Wang, K. Wojciechowski and W. Zhang, *J Phys Chem Lett*, 2014, **5**, 1511-1515.